NEUROSCIENCE

Prolactin-sensitive olfactory sensory neurons regulate male preference in female mice by modulating responses to chemosensory cues

Mari Aoki[1†], Igor Gamayun[1], Amanda Wyatt[1], Ramona Grünewald[1], Martin Simon-Thomas[1], Stephan E. Philipp[1], Oliver Hummel[2], Stefan Wagenpfeil[3], Kathrin Kattler[4], Gilles Gasparoni[4], Jörn Walter[4], Sen Qiao[1], David R. Grattan[5], Ulrich Boehm[1]*

Chemosensory cues detected in the nose need to be integrated with the hormonal status to trigger appropriate behaviors, but the neural circuits linking the olfactory and the endocrine system are insufficiently understood. Here, we characterize olfactory sensory neurons in the murine nose that respond to the pituitary hormone prolactin. Deletion of prolactin receptor in these cells results in impaired detection of social odors and blunts male preference in females. The prolactin-responsive olfactory sensory neurons exhibit a distinctive projection pattern to the brain that is similar across different individuals and express a limited subset of chemosensory receptors. Prolactin modulates the responses within these neurons to discrete chemosensory cues contained in male urine, providing a mechanism by which the hormonal status can be directly linked with distinct olfactory cues to generate appropriate behavioral responses.

INTRODUCTION

Chemosensory cues perceived by sensory epithelia in the nose are important regulators of reproductive physiology and sexual behavior in mice (*1*–*3*). The sense of smell also plays a crucial role in mate recognition and the initiation of mating (*4*). The nasal sensory epithelia are equipped with a unique molecular repertoire of >1500 chemosensory receptors including odorant receptors (ORs) and vomeronasal receptors (*5*–*7*), trace amine-associated receptors (Taars) (*8*), and formyl peptide receptors (*9*, *10*), with each receptor specialized in detecting different cues. With remarkable specificity, each individual olfactory sensory neuron (OSN) in the main olfactory epithelium (MOE) expresses one allele of either a single *Or* or a single *Taar*. Axons from the OSNs in the MOE project to the main olfactory bulb (MOB), where axons from all of the dispersed OSNs that express the same receptor converge into a few specific glomeruli (*11*). Animals use this glomerular map to discriminate myriads of odorants to perceive the external environment in a highly accurate manner (*12*).

To display behaviors that are appropriate for a specific physiological situation, animals need to integrate external cues with their internal hormonal state (*3*, *13*, *14*). This is particularly important in females, which experience markedly fluctuating hormone levels across their life cycle, associated with marked hormone-induced changes in behavior. For example, the regular cyclical changes in hormones during the estrous cycle in rodents are also associated with substantial changes in how a female will interact with a male (*15*). These changes culminate in the expression of estrous behavior, with females only becoming sexually receptive to males for a short period of time following ovulation. During this time, females will exhibit enhanced interest toward males, remaining in close proximity with them and initiating copulation (*16*, *17*). This change may require hormone-induced changes in olfactory processing of male-specific cues, and the specific timing raises the possibility that such a change will be driven by the same hormonal changes that drive ovulation.

The key hormonal event driving ovulation is a sustained increase in estradiol from the developing ovarian follicle during the proestrous period. One consequence is an estradiol-induced surge in the secretion of the pituitary hormone prolactin (*18*), and this proestrous prolactin surge has been implicated in promoting the expression of female sexual receptivity to males (*19*, *20*). Prolactin is highly sexually dimorphic in the mouse, with levels in the female being up to 10-fold higher than seen in males. Females also experience dynamic fluctuations in prolactin associated with the estrous cycle, pregnancy, and lactation (*21*, *22*), and we have shown that prolactin action is critical to some of the profound behavioral changes that occur at this time, such as maternal behavior (*23*). Recent data show that prolactin is also involved in sex-specific sensitization of specific somatosensory pathways associated with nociception (*24*), providing precedent for a role in hormone-induced adaptations of sensory processing. We have recently identified prolactin-sensitive cells in the MOE and in the neuroepithelium of the vomeronasal organ (VNO) of prolactin receptor (Prlr) reporter mice (*25*), potentially enabling prolactin to serve as the estrous cycle–specific signal to regulate olfactory processing of male-specific chemosensory cues. The aim of the present study was to test this hypothesis, by investigating the role of prolactin in regulating function of these critical olfactory and pheromonal sensory structures.

RESULTS

Prolactin increases male preference in female mice

To determine the physiological role of prolactin action in the sensory epithelia of the nose, we generated mice that lack the Prlr specifically in these cells. To do this, we crossed animals carrying a floxed

[1]Department of Pharmacology, Center for Molecular Signaling (PZMS), Saarland University School of Medicine, Homburg, Germany. [2]Faculty of Computer Science, Mannheim University of Applied Sciences, Mannheim, Germany. [3]Institute for Medical Biometry, Epidemiology and Medical Informatics, Saarland University School of Medicine, Homburg, Germany. [4]Department of Genetics, Saarland University, Saarbrücken, Germany. [5]Centre for Neuroendocrinology and Department of Anatomy, School of Biomedical Sciences, University of Otago, Dunedin, New Zealand.
*Corresponding author. Email: ulrich.boehm@uks.eu
†Deceased.

Prlr allele (*26*) with a nasal sensory neuron–specific Cre driver line [olfactory marker protein (OMP)–Cre] (*27*) to generate conditional olfactory *Prlr* knockout (Prlr-cKO) mice. Cre recombinase–mediated inversion of the floxed exon, which inactivates the *Prlr* gene in these animals, was confirmed by polymerase chain reaction (PCR) (fig. S1).

Numerous chemosensory cues that are important for reproductive physiology and sexual behavior have been identified in male urine (*28*–*33*). We therefore initially focused our functional analyses on female responses toward male urine. To do this, we first performed a two-choice preference test using male or female urine in a three-compartment cage (Fig. 1A). The compartments were separated by small walls, but the animals could freely enter any compartment. Females at diestrus (in which prolactin levels are low) were injected with saline or prolactin intraperitoneally before the behavioral tests to mimic a "proestrous-like" prolactin surge in females. A female was first habituated in an empty three-compartment cage for 10 min. None of the groups, regardless of genotype or injection, showed any spatial preference during habituation (fig. S2). After this acclimatization period, male or female urine on a piece of filter paper was introduced into the left or right compartment, respectively, and the behavior of the female was observed (Fig. 1B). The time spent in each compartment was quantified for 10 min (Fig. 1, C and D), and a preference index was calculated by dividing time spent in the left compartment by that spent in the right compartment (Fig. 1, E and F). During test sessions, saline-injected virgin control and Prlr-cKO females showed no preference toward either male or female urine (Fig. 1, C and E). After prolactin treatment, however, control females displayed an enhanced preference toward male urine (Fig. 1, B, D, and F). This effect of prolactin was completely prevented in Prlr-cKO mice, as shown by the significant reduction of time spent with the male urine by Prlr-cKO mice compared with control animals (Fig. 1, D and F). This suggests that the prolactin-induced enhancement of male preference was mediated specifically by prolactin action on sensory neurons in the nose. To examine whether mate preference during endogenous rises in prolactin at proestrus is also impaired in Prlr-cKO females, we next quantified and compared time that females spent with either a male or a female by placing both into the three-compartment test with the experimental female but within a mesh box that allowed olfactory communication but prevented physical interactions (Fig. 1G). We found that control proestrous females spent significantly more time investigating a male compared to Prlr-cKO females (Fig. 1, H and I), indicating that endogenous prolactin regulates the olfactory preference to spend time associating with males during proestrus.

Loss of prolactin-induced male preference in olfactory-specific Prlr knockout females

To investigate whether this altered olfactory preference in Prlr-cKO females affected reproductive behaviors and social interactions with male mice, we used two different two-compartment paced-mating chambers (*34*, *35*). One chamber contained a 10-cm tall divider wall, whereas the other chamber had a 40-cm tall divider wall with two small holes at the bottom (Fig. 1, J and K). Because of the difference in body size between males and females, males were neither able to climb the 10-cm wall nor pass through the holes, while females could freely escape from and come back to the male compartment. Hence, these tests not only evaluated whether females choose to spend time with the male but also assessed whether they actively choose to avoid the males. Prlr-cKO females did not show spatial preferences during habituation (fig. S3). Time that saline-injected control females spent with a male was comparable to that of Prlr-cKO (Fig. 1, L and N). However, following prolactin treatment at diestrus, control females showed more interest in a male and stayed 1.4 times (Fig. 1, L and M, 10-cm divider) and 2 times (Fig. 1, N and O, divider with holes) longer in the compartment containing the male compared to those with saline injection [71.5 s versus 98.0 s (a 10-cm divider; Fig. 1, L and M) and 89.8 s versus 179.5 s (a divider with holes; Fig. 1, N and O, and movies S1 and S2)]. In contrast, prolactin treatment did not affect behaviors in Prlr-cKO females, and they typically chose to escape from the male quickly and spent significantly less time with a male (Fig. 1, M and O, and movies S3 and S4). To examine whether elevated prolactin affects olfactory-mediated mating preferences in intrinsic physiological conditions, we compared females at proestrus, which have high endogenous prolactin levels, with those at diestrus with low prolactin. We found that whereas control females at proestrus exhibited a strong interest in males and spent more time in the male compartment, Prlr-cKO females at proestrus avoided males (Fig. 1, P to S). There was a significant difference between control females at proestrus (with high prolactin) and Prlr-cKO females, suggesting that endogenous prolactin action in the nose enhances interest toward males.

The behavioral differences appeared to be specific to social interactions with males or male urine and not caused by any other effects on locomotion or mood. Prlr-cKO females showed similar locomotor activities in an empty cage when compared to controls (fig. S4, A and B). Prlr-cKO females also investigated peanut butter, a widely used attractant (*36*), for a comparable time to controls, arguing that Prlr-cKO females are still capable of discriminating odorant cues (fig. S4, C and D). To rule out the possibility that the observed male preference effect was due to altered anxiety levels, we placed these females in an elevated plus maze and quantified the time spent and the number of entries into the closed arms. We did not find any altered anxiety-related behaviors in Prlr-cKO females (fig. S4, E and F). Collectively, our behavioral experiments demonstrate a loss of social olfactory preference in Prlr-cKO females. This suggests that prolactin enhances the preference toward males by modulating neuronal activities in the nasal sensory epithelia, resulting in increased attraction toward males during stages of the estrous cycle appropriate for mating.

Prolactin-sensitive OSNs, but not vomeronasal sensory neurons, respond to male urine

Because the conditional knockout strategy targeted Prlrs in sensory neurons of both the MOE (OSNs) and the VNO [vomeronasal sensory neurons (VSNs)], we next aimed to determine which of these two prolactin-sensitive cell populations mediated control of this olfactory social preference. To do this, we functionally examined whether $Prlr^+$ OSNs (Prlr-OSNs) respond to chemical cues in urine by generating mice that express the genetically encoded Ca^{2+} indicator GCaMP3 specifically in the $Prlr^+$ nasal sensory neurons. To do this, we crossed the Prlr-IRES-Cre mice with a Cre-dependent GCaMP3 reporter mouse line (*37*) and then used a confocal Ca^{2+} imaging setup to image turbinates, which are protrusions of the MOE, from females. Male urine applied from a pipette induced an increase in $[Ca^{2+}]_i$ in 36.1% (52 of 144 cells from seven females) of female Prlr-OSNs (Fig. 2, A and B, and fig. S5). The same population of cells was activated again by a second urine application, demonstrating that the Prlr-OSNs reliably respond to repetitive stimulation with chemosensory cues in the same animals or across animals (Fig. 2A).

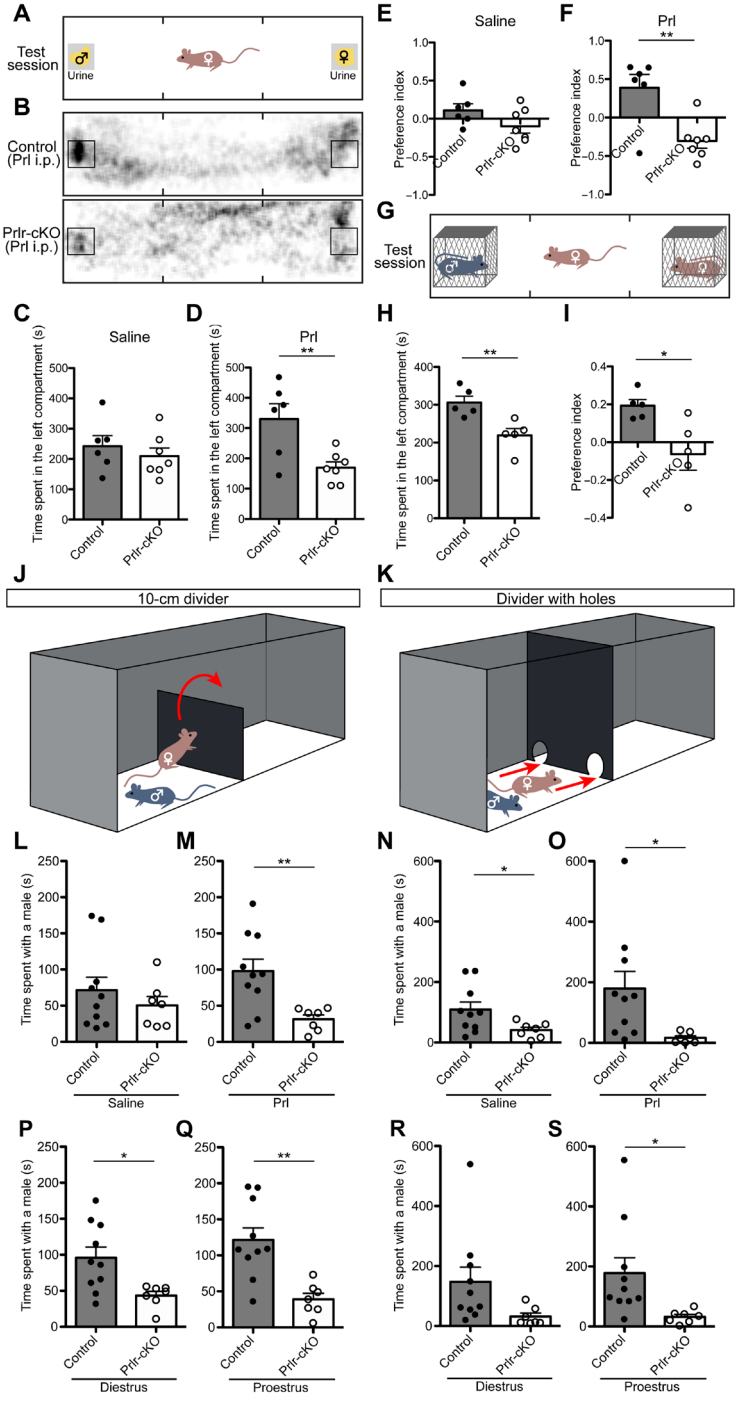

Fig. 1. Loss of social preference in conditional olfactory Prlr-knockout females. (**A**) Two-choice preference tests were performed in a three-compartment cage. After 10-min habituation, pieces of filter paper with male and female urine were placed in the left and right compartment, respectively. i.p., intraperitoneally. (**B**) Representative movement traces of Prl-injected control and Prlr-cKO females in the three-compartment cage during test sessions. (**C** and **D**) Time that control and Prlr-cKO females with saline (C) or prolactin (D) injection spent in the left compartment during test sessions. (**E** and **F**) Preference toward the left compartment (male urine) over the right compartment (female urine) during test sessions. $n = 6$ for controls and $n = 7$ for cKOs. (**G**) Two-choice preference tests performed with a male (left) and a female (right) in mesh boxes. (**H**) Time that control and Prlr-cKO females at proestrus spent in the left compartment. $n = 5$ for controls and cKOs. (**I**) Preference toward the left compartment (a male) over the right compartment (a female). $n = 5$ for controls and cKOs. (**J** and **K**) Social preference of females in a paced-mating chamber separated into two compartments by a 10-cm divider (J) or a divider with small holes (K). (**L** to **O**) Time that control and Prlr-cKO females at diestrus spent in the male compartment after saline (L and N) or prolactin (M and O) injection in a paced-mating chamber with a 10-cm divider (L and M) or a divider with holes (N and O). (**P** to **S**) Time that females at diestrus (P and R) or proestrus (Q and S) spent in the male compartment of a paced-mating chamber with a 10-cm divider (P and Q) or a divider with holes (R and S). $n = 10$ for controls and $n = 7$ for cKOs. Asterisks show significant differences [*$P < 0.05$ and **$P < 0.01$; $P = 0.0090$ (D), $P = 0.0039$ (F), $P = 0.0083$ (H), $P = 0.0219$ (I), $P = 0.0059$ (M), $P = 0.0309$ (O), $P = 0.0131$ (P), $P = 0.0016$ (Q), and $P = 0.0324$ (S)] based on the two-tailed t test (C to F, H, I, and L to S). Error bars show average ± SEM.

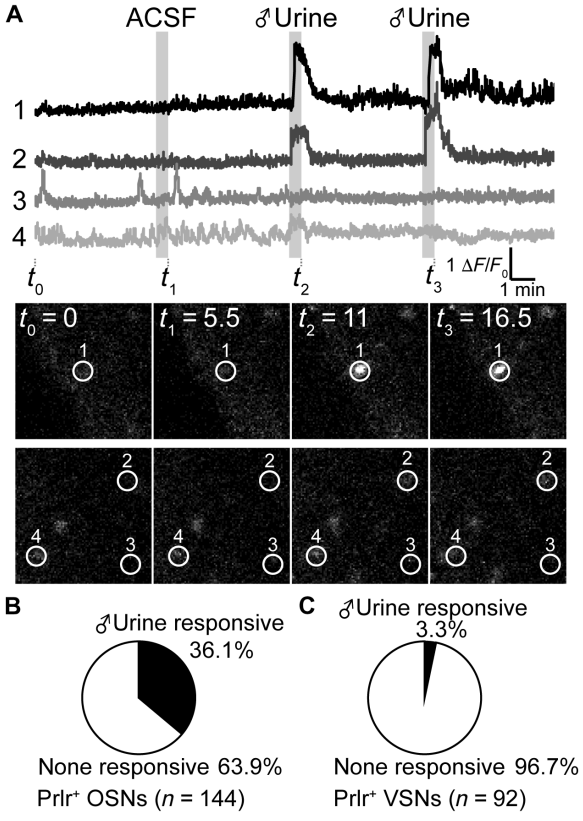

Fig. 2. Female Prlr-OSNs respond to male urine. (**A**) Representative calcium traces of Prlr-OSNs using calcium imaging in Prlr-GCaMP3 females (top). Still frames at $t = 0$ (5 min before ACSF application), $t = 5.5$ (ACSF application), $t = 11$ (first male urine application), and $t = 16.5$ (second male urine application) are shown (bottom). (**B**) Responsiveness of Prlr$^+$ OSNs to male urine application. $n = 144$ (seven females). (**C**) Responsiveness of Prlr$^+$ VSNs to male urine application. $n = 92$ (three females).

Artificial cerebrospinal fluid (ACSF) application did not activate these cells, arguing against a nonspecific activation through mechanical stimuli delivered by the pipette (Fig. 2A). Female Prlr-OSNs also responded to female urine, however, to a lesser extent (fig. S5). In contrast, the vast majority of Prlr-expressing cells in the VNO did not respond to male urine (96.7%, 89 of 92 cells from three females; Fig. 2C), suggesting that, unlike Prlr$^+$ cells in the MOE, prolactin-sensitive VSNs do not make a major contribution to detecting male urine and to social olfactory preference.

Prlr-OSNs project to distinct ventral and dorsal glomeruli in the MOB

To further characterize the prolactin-sensitive OSNs, we generated Prlr–green fluorescent protein (GFP) reporter mice by crossing the Prlr-IRES-Cre mouse line with GFP reporter animals (*38*), giving us genetic access to these cells (*23*, *25*, *39*). The GFP-labeled (GFP$^+$) cells were scattered throughout the MOE without apparent cell clusters (Fig. 3A). Prlr expression in the MOE started at embryonic day 12.5 (fig. S6A). The number of Prl-sensitive cells in the MOE increased substantially from 1.2 ± 0.2 cells/mm^2 in embryos to 72 ± 7.5 cells/mm^2 in adults, comprising ~0.35% of all OSNs (Fig. 3B). This percentage corresponds to that of Prlr$^+$ cells found in an external dataset of a single-cell RNA sequencing [RNA-seq; GSE151346; (*40*)]. In that study, *Prlr* was expressed in 0.33% of *Omp*$^+$ (delineates OSNs) OSNs (70 of 21,195 cells), a percentage highly comparable to our data, suggesting that most, if not all, GFP$^+$ OSNs in our study are likely to acutely express *Prlr*. We found similar numbers of GFP$^+$ cells when comparing male and female animals at every stage analyzed, indicating that Prlr expression in the MOE is invariant between the sexes (fig. S6B).

We next dissociated the MOE of Prlr-GFP females and performed reverse transcription PCR (RT-PCR) on fluorescence-activated cell sorting (FACS)–enriched GFP$^+$ cells using primers specific for *Prlr*, *GFP*, *Omp*, and β-*actin* (*Actb*) (Fig. 3C). Whereas *Omp* was expressed abundantly both in GFP$^+$ and GFP$^-$ control samples, *Prlr* (and *GFP*) mRNA was only detected in the GFP$^+$ fraction, confirming acute *Prlr* expression in these cells. In situ hybridization with an *Omp* probe on MOE sections of Prlr-GFP females showed that GFP expression in the olfactory epithelium was restricted to a subset of *Omp*$^+$ OSNs (Fig. 3D). Representative GFP$^+$ neurons in the MOE shown in Fig. 3D displayed a typical OSN-like cellular morphology with a dendrite extending into the nasal cavity, an *Omp*$^+$ cell body, and an axon projecting to the MOB. Axons of OMP$^+$ OSNs were found in all glomeruli within the MOB, but axon terminals of Prlr-OSNs selectively innervated just a few glomeruli, suggesting that these cells express only a restricted repertoire of *OR* genes (Fig. 3E). OSNs are classified into four zones depending on their dorsoventral localization in the MOE, and they project their axons to the corresponding zones in the MOB (*41*–*44*). The Prlr-OSNs were found in all zones in the MOE, and innervated both dorsal and ventral glomeruli in the MOB, as shown by staining using antibodies against OSN subtype marker proteins delineating dorsal (i.e., zone I) OSNs [olfactory-specific medium-chain acyl coenzyme A (CoA) synthetase (OMACS) (*45*) and NAD(P)H quinone oxidoreductase 1 (NQO1) (*46*)] or ventral (i.e., zones II to IV) OSNs [neuropilin2 (Nrp2) (*47*) and olfactory cell adhesion molecule (OCAM) (*48*)] (Fig. 3E and fig. S7). These data demonstrate that the Prlr-OSNs represent a distinct subset of OSNs in the MOE comprising a limited distribution of both ventral and dorsal glomeruli. We did not find any GFP$^+$ cells in granule cell (interneuronal), mitral/tufted cell, external plexiform, and glomerular layers of the MOB (Fig. 3F), indicating that only the primary sensory neurons in the olfactory system are prolactin sensitive.

A map of Prl-sensitive glomeruli in the brain

Each OSN expresses only a single chemosensory receptor out of a potential repertoire of ~1500 genes, and axons from neurons expressing the same receptor converge in the same glomeruli in the MOB. Although the position, number, and size of glomeruli expressing a given OR vary minimally, the axonal convergence of OSNs is principally hardwired (*49*–*52*). To examine the Prlr-OSN projection pattern in different individuals, we visualized the axonal projections of Prlr-OSNs in whole-mount olfactory bulb preparations by generating mice that express τlacZ specifically in these cells. The τlacZ reporter protein is actively transported down microtubules toward axon terminals, efficiently tracing OSN projections (*53*). We found that the Prlr-OSN axons converge into 95 to 100 of ~4000 glomeruli (*54*) on each hemisphere (right lateral, 52 ± 1.8; right medial, 48 ± 3.6; left lateral, 48 ± 3.0; left medial, 48 ± 4.4; $n = 8$ females). While we noted that some glomeruli were sparsely innervated by Prlr-OSNs, which may account for the higher number of Prlr$^+$ glomeruli than those expected from the percentage of Prlr$^+$ OSNs, the majority were heavily innervated, supporting the concept of a

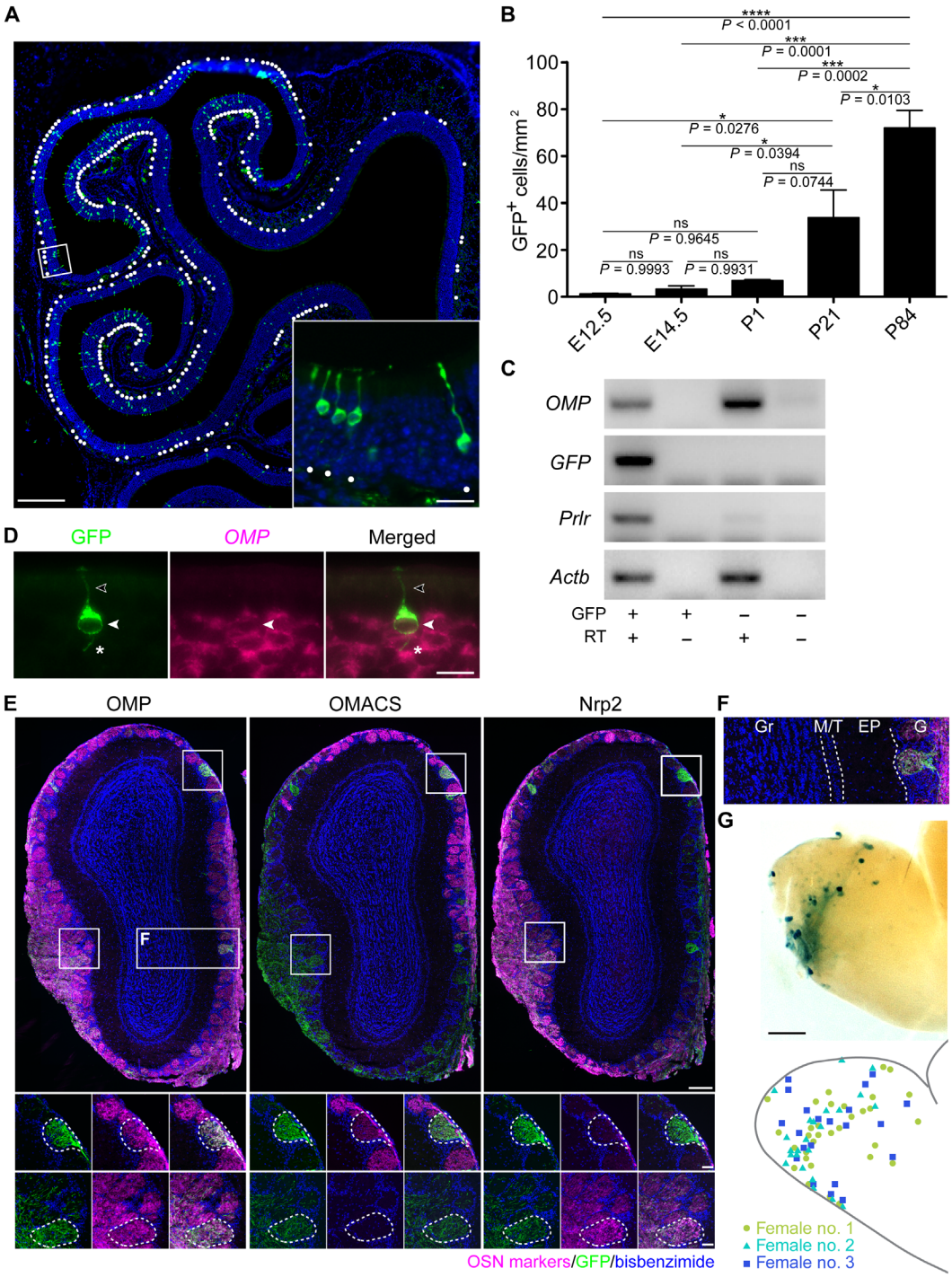

Fig. 3. A map of Prlr-glomeruli in the MOB. (**A**) GFP$^+$ cells (green) in Prlr-GFP mice MOE. Nuclei counterstained with bisbenzimide (blue). White dots demarcate GFP$^+$ cell positions. Scale bars, 200 (overview) and 20 μm (inset). (**B**) Normalized quantification of GFP$^+$ cells from female Prlr-GFP MOE. GFP$^+$ cells at embryonic day 12.5 (E12.5), E14.5, postnatal day 21 (P21), and P84 normalized to MOE area. Shown as means ± SEM. Asterisks depict significance (*P < 0.05, **P < 0.01, and ***P < 0.001) based on one-way analysis of variance (ANOVA) and Tukey's multiple comparison test. ns, not significant. n = 3 per group. (**C**) RT-PCR on cDNA from female Prlr-GFP FACS-sorted GFP$^+$ and GFP$^-$ cells. (**D**) *Omp* probe in situ hybridization on female Prlr-GFP MOE sections. Black arrowheads, white arrowheads, and asterisks indicate dendrite, cell body, and axon, respectively. Scale bar, 10 μm. (**E**) Dual immunolabeling for GFP (green) and OSN markers; OMP, OMACS, and Nrp2 (magenta) on adjacent MOB sections. Nuclei counterstained with bisbenzimide (blue). Scale bars, 200 (overview) and 50 μm (inset). (**F**) Granule cell (Gr), mitral/tufted cell (M/T), external plexiform (EP), and glomerular (G) layers are devoid of GFP$^+$ cells. (**G**) Whole-mount X-gal staining showing LacZ expression in female Prlr-τlacZ lateral MOB (top). Glomeruli positions are summarized for three females (bottom). Scale bar, 500 μm.

controlled projection of Prlr-OSNs within a predetermined glomeruli map. Most Prlr$^+$ glomeruli were found at similar positions within the previously reported interglomerular distances [1.5 to 3 mm; (*50*)] in all individuals examined (Fig. 3G and fig. S8), indicating that Prlr-OSNs express specific ORs/TAARs. Because the OSN population is constantly renewed throughout the life span of the animal (*55*–*57*), the constant percentage of Prlr-OSNs and the similar positions of the Prlr-glomeruli (τlacZ$^+$) in different animals strongly suggest that the Prlr-OSNs constitute a specific subpopulation of OSNs that express a predetermined set of chemosensory receptors. This expression pattern suggests that prolactin is likely to influence responses to a limited set of olfactory cues.

Prlr-OSNs express distinct chemosensory receptors

To identify the chemosensory receptor(s) expressed in Prlr-OSNs, we built three independent RNA libraries from FACS-enriched GFP$^+$ cells prepared from the MOE of three Prlr-GFP females and performed RNA-seq (*58*). Pearson's correlation coefficient analysis confirmed that these biological replicates are reproducible (r = 0.953, r = 0.954, and r = 0.964 for female nos. 1 and 2, nos. 2 and 3, and nos. 1 and 3, respectively). Using this approach, we found high expression values [fragments per kilobase of exon model per million reads mapped (FPKM)] for *Omp* and key olfaction signal transduction genes downstream of ORs and Taars including guanine nucleotide–binding protein G alpha stimulating, olfactory type (*Golf* or *Gnal*), adenylate cyclase type 3 (*Adcy3*), cyclic nucleotide–gated channel alpha 2 (*Cnga2*), and calcium-activated chloride channel anoctamin 2 (*Ano2*) (Fig. 4A). We identified a number of chemosensory receptors that were highly expressed in Prlr-OSNs (Fig. 4B). Only two chemosensory receptors showed mean FPKM values from three biological replicates higher than 100, and 18 receptors showed FPKMs higher than 40 (Fig. 4B, inset). Furthermore, *Olfr1348*, which showed the highest expression among *Ors* and *Taars* in our dataset, was the second most frequently detected *Or* in Prlr$^+$/OMP$^+$ cells from an external single-cell RNA-seq dataset [GSE151346; (*40*)], whereas it showed only 16th (*59*) or 57th [GSE112352; (*60*, *61*)] highest FPKMs of *Ors* and *Taars* found in a bulk RNA-seq dataset of the entire MOE cell populations (Fig. 4C). Likewise, *Olfr1428* and *Olfr672*, which showed the second and third highest FPKM values in Prlr$^+$ OSNs, were ranked at 70th and 21th in the bulk RNA-seq (GSE112352), respectively. This enrichment of specific receptors in the Prlr-OSNs relative to the wider population of OSNs indicates expression of a distinct set of chemosensory receptors within Prlr-OSNs.

Prolactin modulates olfactory detection

To corroborate the RNA-seq data, we then examined the expression of selected *Ors* and *Taars* by in situ hybridization on female MOE sections and found that these chemoreceptors were coexpressed with the Prlr in these OSNs (Fig. 4D). Of the 18 identified chemosensory receptors with mean FPKM values >40, 6 were tested by in situ hybridization and all colocalized with GFP cells (Fig. 4D). Specifically, we found 14.9, 3.3, 6.3, 10.3, 14.7, and 13.7% of the *Olfr672*, *Olfr1348*, *Olfr131*, *Olfr1222*, *Olfr794*, and *Olfr1428* positive OSNs, respectively, to be colocalized with GFP. We also tested four additional ORs that our RNA-seq dataset suggested would not be expressed (FPKM, <1), and none of those colocalized with GFP cells (fig. S9). While most ORs and Taars identified in our screen were orphan receptors, several ligands for Taar3, which is expressed in some Prlr-OSNs (fig. S10), have previously been identified (*8*, *62*).

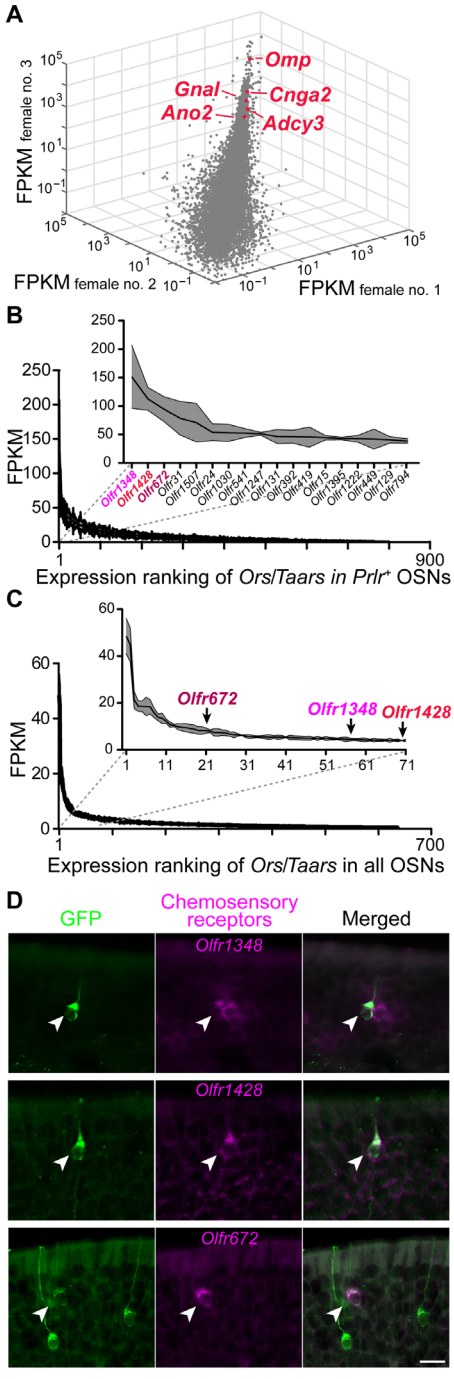

Fig. 4. A distinct set of chemosensory receptors is expressed in Prlr-OSNs. (**A**) FPKM values of RNA-seq data from three different Prlr-GFP females. FPKM values >1 × 10^{-2} are shown. Several key olfactory signal transduction genes [*Cnga2* (cyclic nucleotide–gated channel alpha 2), *Gnal* (guanine nucleotide–binding protein G(olf) subunit alpha), *Adcy3* (adenylate cyclase type 3), and *Ano2* (anoctamin 2)] displayed high FPKM values. (**B**) FPKMs of *Ors* and *Taars* found in the Prlr-OSNs were plotted from the most abundant to the least. Mean of FPKMs from three replicates (line) and the SEM (filled) are shown. *Ors* and *Taars* with FPKMs higher than 40 were shown in the inset. (**C**) FPKMs of *Ors* and *Taars* found in all OSNs from an external bulk RNA-seq (GSE112352) were plotted from the most abundant to the least. FPKMs for top 71 genes were shown in inset. (**D**) In situ hybridization with probes for *Ors* on MOE sections from Prlr-GFP females. *Olfr1348*, *Olfr1428*, and *Olfr672* (magenta) were coexpressed with Prlr/GFP (green) (white arrowheads). Scale bar, 10 μm.

One Taar3 ligand, isopentylamine (IPA; also called isoamylamine), is known to affect reproductive physiology and is also enriched in male urine. In addition, its concentration is reduced in urine from castrated males (*32*). This gave us an experimental tool to dissect Prlr$^+$-OSN signaling in response to a specific chemical and enabled us to analyze the modulation of this signaling by prolactin. IPA was applied via pipette onto MOE tissue from Prlr$^+$-GCaMP3 female mice. We were interested whether prolactin changes the response to IPA; therefore, we chose female mice in diestrus to keep the endogenous prolactin level low. Responses to 100 nM IPA followed by application of prolactin (500 mg/ml) and the combination (IPA + prolactin) were recorded via confocal Ca^{2+} imaging (Fig. 5A). In total, signals from 192 Prlr$^+$-GCaMP3 neurons from seven females were collected for the following response analysis. We took time frames around the application moments and compared the elevation of Ca^{2+} signals 15 s before and after application of different substances (Fig. 5B). Analysis of the difference in the fluorescent *z* score before and after application (ΔFluorescent *z* score) showed that prolactin modulated the IPA responses [see scattering in three-dimensional (3D) plot; Fig. 5C]. We found that the Prlr$^+$-GCaMP3 neurons could be gathered into six clusters, based on correlation between ΔFluorescent *z* scores for each application (Fig. 5C; correlation heatmap based on the triplets of responses for IPA, prolactin, and IPA + prolactin for each neuron, seen in the heatmap for ΔFluorescent *z* scores). Furthermore, it appeared that the clusters were represented by linear regression in certain directions. On the basis of linear fit, calculated as first principal component, we identified the main types of responses to all three applications (Figs. 5C and 3D, plot, fit lines). However, we also found that many of the ΔFluorescent *z* scores are scattered around the origin, depicting either very weak responses or the absence of a response to the applications. To enable a better estimation of the percentage of neurons in the clusters, we set a cutoff based on the distribution of ΔFluorescent *z* scores for the control application (cutoff 95% quantile, *z* score histogram; Fig. 5C). Thus, we found that 42% of neurons showed responses above the cutoff (Fig. 5D). Among them, 4% of all neurons had responded only to prolactin and had no response to IPA (Fig. 5, green cluster). An inhibitory effect of prolactin was seen in 19% of neurons, which responded to IPA, but not to prolactin, and then showed no response to the combination of prolactin + IPA. Another 3% not only had very weak responses to IPA or prolactin but also lacked prolactin + IPA responses (dark blue and orange clusters). In contrast, potentiating effects of prolactin were seen in 3% of neurons that responded to IPA and not to prolactin but had stronger responses when prolactin + IPA were added in combination. In a further 8%, neither IPA nor prolactin evoked a response, but prolactin + IPA administration gave strong responses (maroon and light blue clusters). Five percent of neurons responded to prolactin but showed no response to prolactin + IPA or to IPA alone (magenta cluster), showing the ability of IPA to also modify prolactin responses. Together, these data demonstrate that prolactin modulates the detection of an olfactory signal.

DISCUSSION

Olfaction is the most important sensory modality for rodents to communicate with conspecifics and trigger physiological changes and social/reproductive behaviors (*1*). Here, we document the unexpected finding that elevated prolactin can alter the response to specific olfactory cues and that this effect contributes to females increasing preference to associate with males at a specific time during their reproductive cycle. The presence of hormone receptors in the MOE is not unprecedented, with receptors such as those for the sex steroids progesterone and estradiol already characterized within the MOE (*3*, *63*). Those receptors are broadly expressed throughout the nasal sensory epithelia, however, suggesting that the hormonal ligands affect most, if not all, sensory neurons in these tissues. The intriguing feature of the identified nasal prolactin system is that expression of its receptor is limited to selected OSNs (~0.35% of all sensory neurons in the MOE) coupled with only a restricted subset of ORs, meaning that these Prlr-OSNs are wired to converge to a few distinct glomeruli. This enables prolactin to specifically modulate the perception of a limited group of olfactory cues to influence specific behaviors that may be appropriate only at a particular hormonal state. Fine-tuning by a small population of neurons is especially important for olfactory perception, as widespread regulation of OSNs can actually lead to impaired olfactory discrimination because all neurons are influenced at the same time [analogous to mice expressing the OR M71 in >95% OSNs, which cannot detect the M71 ligand, when most glomeruli are activated (*64*)]. We note that some glomeruli are densely and others are sparsely innervated by Prlr-OSNs, suggesting that the strength of prolactin action on each glomerulus may vary. One important caveat is that the Prlr is also expressed in a few sensory neurons in the VNO (*25*). Because the OMP-Cre also deletes there, we cannot rule out the possibility that these Prlr$^+$ cells may contribute to the behavioral phenotype observed in the cKO females. However, our calcium imaging data showed that only ~3% of Prlr$^+$ neurons in the female VNOs responded to male urine, suggesting that Prlr in the MOE plays a more dominant role in the induction of male preference in females.

The presence of Prlr in the MOE and the olfactory bulb (OB) was first reported in neonatal rats more than 20 years ago (*65*), but the role of prolactin in this system remains unknown. Prlr expression in the mouse olfactory system has not been reported until our recent work using a genetic reporter system (*25*), and in this model, granule cell (interneuronal), mitral/tufted cell, external plexiform, and glomerular layers of the OB in mice were devoid of GFP signals, suggesting a marked difference between the prolactin-sensitive olfactory system in mice and rats.

While prolactin action in the olfactory system at proestrus may seem unexpected at first sight, since this hormone is typically associated with behavioral changes at other states of high prolactin such as pregnancy and lactation, prolactin has previously been shown to be involved in female reproductive behaviors such as lordosis (*19*). The present data begins to elucidate a neuronal basis for this effect, linking olfactory signals relating to mate choice to the hormone-induced changes in behavior. Given the widespread expression of sex steroid receptors in the OSNs (*3*, *63*) and the interactions between the sex steroids and prolactin signaling in other aspects of biology, it would be interesting to investigate whether prolactin regulation of OSNs is altered under conditions of changing steroid hormones, such as during pregnancy or after menopause. Prolactin might also affect olfaction in central circuits since Prlrs are also expressed throughout many central nervous system structures involved in olfactory responses, including the bed nucleus of the stria terminalis (BNST), amygdala, and medial preoptic area (MPOA) (*23*, *39*). Consistent with this, male odor-induced activation of hypothalamic kisspeptin neurons (which express the Prlr) (*66*) impinges on mate preference and sexual motivation (*67*).

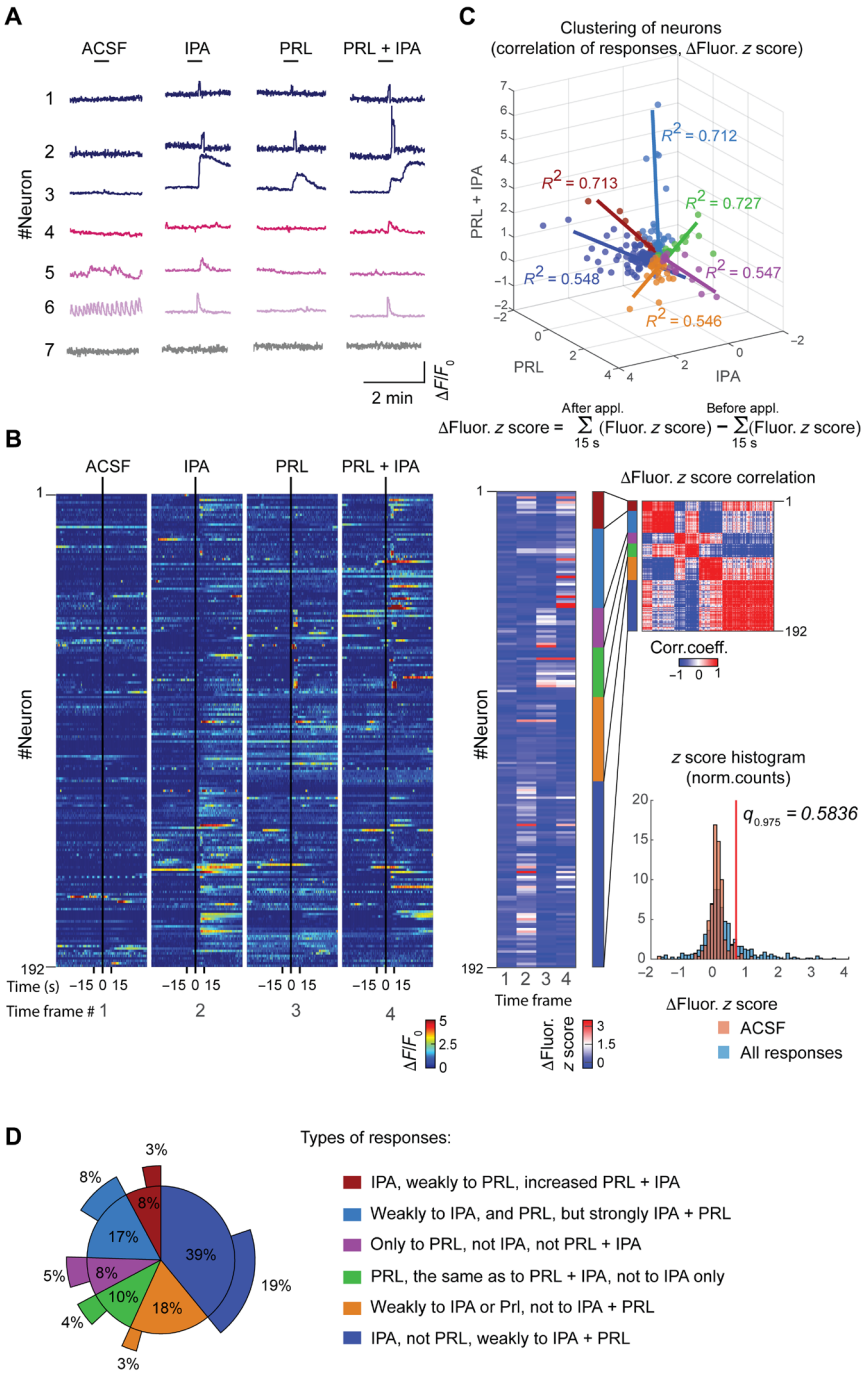

Fig. 5. Prolactin modulation of OSN responses. (**A**) Representative traces of normalized GCaMP3 responses to 100 nM IPA, prolactin (PRL; 500 ng/ml), and combination IPA + PRL. ACSF as control application at the beginning of measurements. (**B**) Heatmaps of normalized fluorescence intensities from 192 neurons. Vertical lines show corresponding substance application. Bottom: Time periods taken for Ca^{2+} response analysis (15 s before and after substance application). Time frame number indicates each different substance application. Neuron presentation order in the heatmaps was changed according to analysis of Ca^{2+} responses from (C). (**C**) Ca^{2+} response analysis. Neurons were clustered by their correlation of responses to IPA, PRL, and PRL + IPA. (C) Top: 3D plot of the ΔFluorescent *z* scores from 192 neurons (calculated with the central formula; applied substances indicated on the 3D plot axes). One circle represents each neuron, collected into clusters (color coded). For every cluster, the corresponding line and coefficient of determination (R^2) represents the best linear fit (first principal component) between responses. Clustering based on the correlation matrix [heatmap; (C), middle and right] is presented as a color-coded bar. All the ΔFluorescent *z* scores for all application cases; time frames for ACSF (1), IPA (2), PRL (3), PRL + IPA (4) are seen as a heatmap [(C), left], where 192 neurons were clustered by their responses (color-coded bar). Histogram [(C), bottom and right] shows normalized ΔFluorescent *z* scores to ACSF and all responses (IPA, PRL, and PRL + IPA values collected together). The 95% quantile (red line, $q_{0.975}$, for ACSF distribution) was taken as a cutoff for "significant" responses. (**D**) Response variability. Pie chart (inner circle) shows percentage of neurons responding to IPA, PRL, and IPA + PRL [types of responses are listed on the right; color-coding matches clustering from (C)]. Pie chart outer sectors show percentage of neurons with responses above the cutoff [compared to control (ACSF) responses, determined in (C)].

While the Prlr-OSN system is not sexually dimorphic in terms of Prlr expression, its function is likely to be strongly sexually dimorphic because of the profound sex differences in levels of the ligand (10-fold higher in females, in mice) and in the sex-specific situations where prolactin is elevated such as proestrus (*18*, *21*). Across multiple species, female animals at this reproductively receptive stage display a stronger olfactory preference toward males than those at nonreproductive stages [mice (*16*, *17*), rats (*68*), and dogs (*69*)]. Although vision is the dominant sense in humans, women are also more attracted to male body odor when around ovulation, near the peak fertility of their cycle (*70*–*72*). Our findings suggest that elevated prolactin is a key regulator that coordinates the physiological states with behaviors by modulating olfactory perception.

Considering that females at proestrus or those with prolactin injection were more attracted to males in our behavioral assays, it seems most likely that Prlr$^+$ OSNs are regulated by prolactin of pituitary origin that is circulating via the blood. It is well established that prolactin is transported across the blood-brain barrier to act on Prlrs expressed widely throughout the brain. In addition, intraperitoneal injection of the azo dye Evans Blue, which binds serum albumin and does not cross the blood-brain barrier, stained the MOE, but not the MOB, demonstrating that the blood vessels in the MOE are highly permeable (fig. S11). Hence, prolactin in blood could also diffuse into the MOE to modulate odor-induced OSN activity. However, our findings cannot exclude the possibility that prolactin found in urine is detected by the OSNs by sniffing.

The Prlr-glomeruli are neither evenly nor randomly distributed in the MOB, and the Prlr is coexpressed with a discrete small set of chemosensory receptors in the Prlr-OSNs. At present, it is unclear whether the choice of the chemosensory receptor triggers Prlr expression or vice versa and whether the cells become prolactin sensitive first and then choose one out of only few chemosensory receptor genes to be expressed. The mechanism by which these specific OSNs choose from the repertoire of >1200 *Or* and *Taar* genes encoded in the genome to restrict expression to less than 30 of those genes remains a fascinating question. Upon analyzing the chromosomal localization of these *Or* genes with respect to the Prlr within the genome, we did not find evidence of clustering that could help provide a simple molecular explanation for the observed coexpression.

We have shown that the Prlr is expressed alongside a restricted subset of ORs in the MOE, that this expression is maintained over time despite frequent renewal of the cells, and that this pattern is highly similar between individuals. These Prlr-OSNs respond to direct application of both prolactin and other chemosensory cues, and the specific removal of Prlrs within the olfactory system leads to a loss of male preference observed in states of high prolactin. Together, our study demonstrates that the pituitary hormone prolactin modulates olfactory detection within the nose to trigger behavior appropriate for the internal hormonal state of the animal.

MATERIALS AND METHODS

Animals

Animal care and experimental procedures were performed in accordance with the guidelines established by the animal welfare committee of Saarland University. Prlr-IRES-Cre mice (*23*, *39*) were crossed with ROSA26-CAGS-τGFP reporter animals (*38*) to generate Prlr-IRES-Cre/ROSA26-CAGS-τGFP (Prlr-GFP) mice. Prlr-GFP mice express a tau (τ)–eGFP fusion protein (*73*) in Prlr$^+$ cells following Cre-mediated recombination. Mice were kept under a standard light/dark cycle with food and water ad libitum. For the X-gal staining (Prlr-τlacZ) and calcium imaging (Prlr-GCaMP3), Prlr-IRES-Cre mice were crossed with ROSA26-BL-IRES-τlacZ (*74*) or eROSA26-GCaMP3 (provided by D. Bergles, Johns Hopkins University School of Medicine, USA) (*37*) animals, respectively. OSN-specific Prlr knockout (Prlr-cKO) mice were generated by crossing Prlrlox/lox (*26*) with OMP-Cre mice (provided by P. Mombaerts, Max Planck Research Unit for Neurogenetics, Frankfurt am Main, Germany) (*27*). Faithful recombination of the floxed allele in the Prlr-cKO mice was validated by PCR using primers that detect the inverted sequence [5′-CGTTCGTGGCATTTACTGTGATGA-3′ and 5′-TACAAGG-GTTAGCAGTGAGGGAA-3′; 465 base pairs (bp)]. All mice have a mixed 129 × C57BL/6 genetic background, except for males of the 129S6 strain that were used in behavioral assays.

Tissue preparation

Prlr-GFP males and females were anesthetized with an intraperitoneal injection of ketamine/xylazine and transcardially perfused with saline followed by 4% paraformaldehyde in phosphate-buffered saline (PBS). Olfactory tissues and brain were removed and postfixed overnight in 4% paraformaldehyde in PBS. The olfactory epithelial tissue was placed in 0.5 M EDTA until decalcified (~2 days). Embryos were taken from timed pregnant mothers and placed in 4% paraformaldehyde in PBS overnight. Sexes of the embryos and postnatal day 1 pups were determined by PCR using *SRY* primers (5′-GAGAGCATGGAGGGCCAT-3′ and 5′-CCACTCCTCTGT-GACACT-3′). Following incubation in 30% sucrose in PBS, tissues were frozen in tissue freezing medium (Leica, Nussloch, Germany) in a dry ice/ethanol slurry. Sections (14 μm thick) were cut using a cryostat (Leica) and stored at −80°C until use.

Immunohistochemistry

Sections were washed in PBS and incubated in 5% donkey serum and 0.2% Triton X-100 in PBS for 30 min. Sections were then incubated with antibodies against GFP (chicken; 1:2000; A10262; Invitrogen, Carlsbad, CA, USA; RRID: AB_2534023), OMP (goat; 1:1000; 544-10001; FUJIFILM Wako, Osaka, Japan; RRID: AB_664696), NQO1 (goat; 1:200; catalog no. ab2346; Abcam, Minneapolis, MN, USA; RRID: AB_302995), OMACS [rabbit; 1:400 (*46*); a gift from H. Takeuchi, Graduate School of Pharmaceutical Sciences, University of Tokyo, Tokyo, Japan], Nrp2 (goat; 1:200; catalog no. AF2215; R&D Systems, Minneapolis, MN, USA; RRID: AB_2155371), and OCAM (goat; 1:500; catalog no. AF778; R&D Systems, Minneapolis, MN, USA; RRID: AB_2149710) overnight at 4°C. Following washing with 0.2% Triton X-100 in PBS, sections were incubated with goat anti-chicken Alexa Fluor 488 (1:400; A11039; Invitrogen; RRID: AB_142924), donkey anti-chicken Alexa Fluor 488 (1:400; 703-545-155; Jackson ImmunoResearch, Cambridgeshire, UK; RRID: AB_2340375), donkey anti-rabbit Cy3 (1:400; 711-165-152; Jackson ImmunoResearch; RRID: AB_2307443), and donkey anti-goat (1:400; 705-165-147; Jackson ImmunoResearch; RRID: AB_2307351) for 1 hour at room temperature. Cell nuclei were counterstained with bisbenzimide. Images were captured using either a Zeiss Axio Scan.Z1 slide scanner or a Zeiss Axio Imager2 microscope with a motorized stage, with multiple images combined to form a composite image using the MozaiX module in the AxioVision software (Zeiss, Jena, Germany).

Quantification of GFP$^+$ cells in the olfactory epithelium

Ten representative sections based on similarity in respect to anatomical structure were selected from each animal ($n = 3$), and the number of GFP$^+$ cells per section was counted. The respective area of the MOE was quantified using ImageJ. Statistical analyses were performed using Prism 5 (Graph Pad). One-way analysis of variance (ANOVA) was used, followed by Tukey's multiple comparison test.

Reverse transcription polymerase chain reaction

OSNs from Prlr-GFP females were dissociated using 0.025% trypsin and 0.01% EDTA in PBS (pH 7.4) (Invitrogen). GFP$^+$ and GFP$^-$ cells were then sorted using a BD FACSAria III (Biosciences). RNA from sorted cells was purified using an RNeasy Plus Micro Kit (QIAGEN), and the same amount of RNA was used for cDNA synthesis by SuperScript III (Invitrogen). PCR was performed using primers specific for *Omp*, *GFP*, *Prlr*, and β-*actin* (table S1).

In situ hybridization combined with anti-GFP immunostaining

To prepare RNA probes for in situ hybridization, 300- to 1000-bp DNA fragments of *Ors* were amplified by PCR using primers shown in table S2 and subcloned into the pGEM-T vector (Clontech). DNA templates for *Omp* and *Taar3* probes were prepared using forward and reverse primers containing SP6 and T7 promoter sites, respectively. A digoxigenin (DIG)–labeled RNA probe was prepared using a DIG RNA labeling kit (Roche, Mannheim, Germany). In situ hybridization was performed as described (*75*). Briefly, 10-μm-thick sections were fixed for 15 min in 4% paraformaldehyde in PBS at 4°C. The sections were then rinsed with PBS and subsequently incubated with Proteinase K [7 μg/ml; in 10 mM tris-HCl (pH 7.4) and 1 mM EDTA] for 10 min at 37°C. After fixing with 4% paraformaldehyde in PBS for 10 min, the sections were incubated with 0.25% acetic anhydride and 0.1 M triethanolamine (pH 8.0), washed with PBS, and air-dried. Sections were then incubated for 16 hours at 51°C with the probes in the hybridization buffer. Sections were subsequently washed with 2× SSC/50% formamide, 2× SSC, and 0.2× SSC for 20 min at 65°C. After blocking with the blocking reagent (Roche; RRID: AB_2313639), slides were incubated with alkaline phosphatase–conjugated anti-DIG antibody (Roche) and chicken anti-GFP antibody (Aves Laboratories, Tigard, OR, USA; RRID: AB_2307313). Following the detection of the Riboprobe using HNPP/Fast Red (Roche), sections were incubated with goat anti-chicken Alexa Fluor 488 antibody (1:400; A11039; Invitrogen; RRID: AB_142924). For each *Or* that we investigated by in situ hybridization, we analyzed at least three coronal sections (each covering the entire MOE) taken from throughout the MOE (rostral to caudal) from at least two 12-week-old female mice. In each section, we could identify between 220 and 300 GFP$^+$ OSNs. For *Olfr672*, *Olfr1348*, *Olfr131*, *Olfr1222*, *Olfr794*, and *Olfr1428*, we identified an average of 54, 54, 45, 43, 42, and 37 positive OSNs, respectively, per section. Of these, 14.9, 3.3, 6.3, 10.3, 14.7, and 13.7% were colocalized with GFP. A similar analysis was undertaken for the *Ors* for which no colocalization was found. The average number of cells found to be positive for *Olfr970*, *Olfr341*, *Olfr893*, and *Olfr764* ranged from 12 to 41 per section.

RNA sequencing

GFP$^+$ OSNs from Prlr-GFP females at diestrus ($n = 3$) were sorted using a MoFlo XDP cell sorter (Beckman Coulter, Germany), and RNA from sorted cells was purified using the RNeasy Plus Micro Kit (QIAGEN). DNA libraries were built using the Smart-seq2 method (*48*). Briefly, reverse transcription was performed using a template-switching oligo with SuperScript II (Invitrogen). After the first-strand reaction, the cDNA was preamplified using the KAPA HiFi HotStart ReadyMix (Kapa Biosystems). The amplified samples were then purified using AMPure XP beads (Beckman Coulter). The tagmentation reaction and the amplification of adapter-ligated fragments were performed using the Nextera XT DNA Sample Preparation Kit (Illumina). The amplified samples were then purified using AMPure XP beads, and the quality check was carried out using the Bioanalyzer High Sensitivity DNA Kit (Agilent). Libraries were then sequenced using the Illumina HiSeq 2500 platform (San Diego, CA, USA) with 100-bp single-end reads. After a quality control with FastQC version 0.11.2 (www.bioinformatics.bbsrc.ac.uk/projects/fastqc/), reads were adapter-trimmed ($Q < 20$) with Cutadapt (version 1.4.132) using Trim Galore! version 0.3.3 (www.bioinformatics.babraham.ac.uk/projects/trim_galore/). Reads were aligned to mm10 assembly with the grape-nf pipeline (https://github.com/guigolab/grape-nf) wrapping STAR version 2.4.0j33 (*76*) and RSEM version 1.2.2134 (*77*). Read counts were normalized as FPKM values. Expression of *OR* genes that showed high FPKM values in all three females were then examined by in situ hybridization.

Processed single-cell (GSE151346) (*40*) and bulk (GSE112352) (*60*, *61*) RNA-seq read count matrices were downloaded from the Gene Expression Omnibus (www.ncbi.nlm.nih.gov/geo/). Read counts were normalized using edgeR (*78*) and filtered for unexpressed genes with a cut-off of CPM (counts per million) < 0.5. In the single-cell RNA-seq dataset, Prlr$^+$/OMP$^+$ were defined by Prlr and Omp expression levels of CPM > 0.5. Last, genes were ranked by FPKM values in the individual datasets.

Whole-mount X-gal staining

Brains were dissected from 12-week-old Prlr-τlacZ females ($n = 3$), and X-gal staining was performed as previously described (*53*). After staining, brains were dehydrated with ethanol and cleared with benzyl benzoate:benzyl alcohol (1:1) solution. Images were then photographed using a stereo microscope M205 FA (Leica) and an AxioCam MRc5 camera (Zeiss). The position of glomeruli was traced using Illustrator, and the traces from three females were overlaid to show the summary of the glomerular distribution.

Calcium imaging

Vaginal smears were taken in the morning of the day of the experiment, and only females at diestrus were used for the calcium imaging. Following cervical dislocation, the olfactory tissues were dissected in ice-cold ACSF (125 mM NaCl, 2.5 mM KCl, 1 mM $MgCl_2$, 2 mM $CaCl_2$, 1.25 mM NaH_2PO_4, 25 mM $NaHCO_3$, and 10 mM glucose) and incubated in ACSF at room temperature for at least 30 min. Turbinates of the MOE were then stabilized using 4% TopVision Low Melting Point Agarose (Thermo Fisher Scientific, #R0801) and a custom-made anchor in a recording chamber and perfused constantly with carbogenated ACSF at a rate of 2 ml/min. A total of 333 μl of each stimulus [ACSF, male/female urine (1:100), 100 nM IPA, Prl (500 ng/ml), and 100 mM KCl, diluted in ACSF] was applied from a pipette for 10 s (~2 ml/min) with a 5-min interval of washing in ACSF. The concentration of prolactin was selected on the basis of the previous finding that prolactin application (500 ng/ml) induced an increase in firing in the majority of tuberoinfundibular dopamine

neurons (*79*). Because OSNs have been reported to show stable responses to repetitive stimuli, even after only a 3-min wash interval (*80*–*82*), multiple stimuli were applied sequentially separated by 5-min wash steps. Male and female urine were applied in a random order. IPA, prolactin, the mixture of IPA and prolactin, and KCl were applied sequentially in this order. Calcium imaging was performed using an upright confocal microscope LSM 710 (Zeiss) with excitation light at 488 nm (argon laser) and emission filter at 493 to 598 nm. Images were taken with a frame rate of 2 Hz using a water immersion 20× objective Plan-Apochromat (Zeiss) and ZEN Black software (Zeiss). Fluorescent images underwent spatial movement correction using a custom-written script for MATLAB (R2021, MathWorks, Natick, MA, USA) taken and adjusted from an open source script (https://doi.org/10.1017/S1551929514000790). Fluorescence intensities from selected regions of interest were collected using ImageJ. $\Delta F/F_0 = (F - F_0)/F_0$ was calculated and shown in graphs, where F_0 is the mean fluorescence 1 min before the first application with ACSF and F is the fluorescent intensity of each image. For quantification between different applications, baselines of calcium traces were corrected using MATLAB script Baseline Fit (www.mathworks.com/matlabcentral/fileexchange/24916-baseline-fit; 2009, M. Hrovat). Time frames from 15 s before and to 15 s after corresponding moments of substance application were chosen for further analysis. Then, the differences in z scores (ΔFluorescent z score, calculated as sum of z score after application minus sum of z scores before application; formula shown in figure) were taken as characteristic values of the responses. Heatmaps, z score calculation, correlation clustering analysis, histogram, and percentage quantification were done with MATLAB.

Behavioral analyses

Animals

Urine was collected by applying gentle pressure on the abdomen of the animals. Urine from multiple males (up to five) or multiple females (up to five) at diestrus females was then pooled, aliquoted, stored at −80°C, and thawed shortly before use. Animals had a mixed 129 × C57BL/6 genetic background and were group-housed under an inverted light/dark cycle for >1 week before the experiment. Eight- to 24-week-old *Prlr* fl/fl (controls) and *Prlr* fl/fl, *Omp*-Cre cre/wt (Prlr-cKO) virgin females were used. Vaginal smears were taken in the morning of the day of the experiment to define the estrous stage of the experimental animals. To mimic the prolactin surge, prolactin (5 mg/kg; Sigma and National Hormone and Peptide Program, dissolved in saline) or saline (control) was injected intraperitoneally at diestrus 45 min before the experiment. Using Evans Blue, we confirmed that substances injected intraperitoneally reach the nose 45 min after the injection (fig. S11).

Two-choice preference test

Two-choice preference tests were performed in a three-compartment cage (size of one compartment: 18 cm by 15 cm by 40 cm). The cage is separated into three compartments with small walls, but the animals can freely enter any compartment. After a female was habituated in the empty three-compartment cage for 10 min, 4 cm–by–4 cm filter papers with 100 μl of male and female urine were placed at the left and right side of the cage, respectively. For testing mate preference, a female was placed in the three-compartment cage with a male (left) and a female (right) in metal mesh boxes (7.9 cm by 7.9 cm by 9.5 cm). To investigate whether olfaction in Prlr-cKO females is impaired, two-choice preference tests were performed in a three-compartment cage with 100 μg of peanut butter and 100 μl of water on pieces of filter paper at the left and right of the cage, respectively. Behaviors were recorded for 10 min using a video camera (DCR-SR90E, Sony).

Social preference assay

To examine social preference, custom-made two-compartment paced-mating chambers (size of one compartment, 18 cm by 15 cm by 40 cm) were used, one of which has a 10-cm tall divider and the other has a 40-cm tall divider with two holes (diameter, 2 cm) at the bottom (Fig. 4, J and K). Previous studies showed that a barrier of 10 cm (*34*) or a barrier with 2.54-cm holes (*35*) can restrict a male in a compartment while allowing females to go through the barrier freely. We adjusted the size of holes to a diameter of 2 cm so that we were able to restrict males more efficiently in our experiments. Females at diestrus or proestrus were habituated in empty paced-mating chambers for 10 min, and females that did not cross the divider during habituation were excluded from statistical analyses. They were then placed in the left chamber together with a 20- to 30-week-old sexually experienced wild-type male (genetic background, 129S6), and behaviors were videotaped for 10 min. Brown-coated 129S6 males were used so that they can be visually distinguished from females (129 × C57BL/6, which usually have black coat color) in the following video analyses. Males were used repeatedly up to four times for these tests. As males are larger and heavier than females (*83*), males were neither able to climb the 10-cm wall nor pass through the holes, whereas females could freely escape from and come back to the male compartment. More than 80% of males did not go through the barrier, and the males that went through were eliminated and the behavior session was excluded from the statistics. Females at diestrus were used in the mating chamber behavior assay first as "diestrus" group, and when at proestrus after a minimum 5-day interval from the last behavior assay, they were used as "proestrus" group. When at diestrus after another minimum 5-day interval, they were injected with saline and used as "saline" group and injected with prolactin and used as "Prl" group after another interval. Prolactin was injected at the end to avoid possible interference with reproductive physiology. Vaginal smears were monitored to eliminate pregnant females after the behavior assay with a male. When we compared virgin females (diestrus group) with females that had two assays of social contact with males (saline group), we did not observe obvious learning effects. When comparing females at different stages or with saline/Prl, we found behavioral changes, suggesting that the hormone-induced behaviors override possible learning effects. Statistical analyses were performed using two-tailed t test or one-way ANOVA followed by a Bonferroni's multiple comparisons test.

Elevated plus maze

To examine the anxiety level, animals were placed in an elevated plus maze (width, 7 cm; arm length, 30 cm; and height, 70 cm), and behaviors were recorded for 5 min. The time spent in the closed arms and the entries in closed arms were quantified.

Video analyses of two-choice preference test

Total traveled distance and average speed of movement during habituation were quantified using an ImageJ plugin wrMTrck (*84*, *85*). A custom-made Java script was used to trace the movement of females. Briefly, the program analyzed the video recordings of the mice frame by frame and in good approximation calculated the center point of all pixels whose color value changed between two adjacent frames above a given threshold to locate the mouse in the second of

the two frames. Every time a movement was detected like this, a square of 7 by 7 pixels around this center point was "heated up" from black (0) via dark red to bright red (255) by increasing the brightness of the red channel in the RGB color value for each pixel in this square. The increment was dynamically calculated dependent on the length of the recording to achieve an optimal contrast in the heatmap. The heatmap was then converted to a black and white image, and the color was inverted. Preference indices were calculated using the following equation: *preference index* = $(T_{left} - T_{right})/(T_{left} + T_{right})$, where T_{left} and T_{right} represent time spent in left and right compartment, respectively. Statistical analyses were performed using two-tailed *t* test or one-way ANOVA followed by a Bonferroni's multiple comparisons test.

Intraperitoneal injection of Evans Blue

Evans Blue (2%; dissolved in saline) was injected intraperitoneally in 14-week-old wild-type females (5 ml/kg). Fifteen, 30, 45, and 60 min after the injection, animals were euthanized by cervical dislocation following an overdose of ketamine/xylazine, and the MOE and the OB were dissected. As controls, animals were euthanized 45 min after saline (5 ml/kg) injection, and the olfactory tissues were removed in the same way. Images were then photographed using a M205 FA (Leica) stereo microscope and an AxioCam MRc5 camera (Zeiss).

SUPPLEMENTARY MATERIALS

Supplementary material for this article is available at https://science.org/doi/10.1126/sciadv.abg4074

View/request a protocol for this paper from *Bio-protocol*.

REFERENCES AND NOTES

1. M. Halpern, A. Martinez-Marcos, Structure and function of the vomeronasal system: An update. *Prog. Neurobiol.* **70**, 245–318 (2003).
2. K. Touhara, L. B. Vosshall, Sensing odorants and pheromones with chemosensory receptors. *Annu. Rev. Physiol.* **71**, 307–332 (2009).
3. S. Dey, P. Chamero, J. K. Pru, M. S. Chien, X. Ibarra-Soria, K. R. Spencer, D. W. Logan, H. Matsunami, J. J. Peluso, L. Stowers, Cyclic regulation of sensory perception by a female hormone alters behavior. *Cell* **161**, 1334–1344 (2015).
4. M. J. Baum, J. A. Cherry, Processing by the main olfactory system of chemosignals that facilitate mammalian reproduction. *Horm. Behav.* **68**, 53–64 (2015).
5. L. Buck, R. Axel, A novel multigene family may encode odorant receptors: A molecular basis for odor recognition. *Cell* **65**, 175–187 (1991).
6. G. Herrada, C. Dulac, A novel family of putative pheromone receptors in mammals with a topographically organized and sexually dimorphic distribution. *Cell* **90**, 763–773 (1997).
7. H. Matsunami, L. B. Buck, A multigene family encoding a diverse array of putative pheromone receptors in mammals. *Cell* **90**, 775–784 (1997).
8. S. D. Liberles, L. B. Buck, A second class of chemosensory receptors in the olfactory epithelium. *Nature* **442**, 645–650 (2006).
9. S. Riviere, L. Challet, D. Fluegge, M. Spehr, I. Rodriguez, Formyl peptide receptor-like proteins are a novel family of vomeronasal chemosensors. *Nature* **459**, 574–577 (2009).
10. S. D. Liberles, L. F. Horowitz, D. Kuang, J. J. Contos, K. L. Wilson, J. Siltberg-Liberles, D. A. Liberles, L. B. Buck, Formyl peptide receptors are candidate chemosensory receptors in the vomeronasal organ. *Proc. Natl. Acad. Sci. U.S.A.* **106**, 9842–9847 (2009).
11. P. Mombaerts, Axonal wiring in the mouse olfactory system. *Annu. Rev. Cell Dev. Biol.* **22**, 713–737 (2006).
12. S. DeMaria, J. Ngai, The cell biology of smell. *J. Cell Biol.* **191**, 443–452 (2010).
13. R. E. Whalen, F. Johnson, Individual differences in the attack behavior of male mice: A function of attack stimulus and hormonal state. *Horm. Behav.* **21**, 223–233 (1987).
14. K. S. Lynch, D. Crews, M. J. Ryan, W. Wilczynski, Hormonal state influences aspects of female mate choice in the Túngara frog (Physalaemus pustulosus). *Horm. Behav.* **49**, 450–457 (2006).
15. L. Zinck, S. Q. Lima, Mate choice in Mus musculus is relative and dependent on the estrous state. *PLOS ONE* **8**, e66064 (2013).
16. M. Eliasson, B. J. Meyerson, Sexual preference in female rats during estrous cycle, pregnancy and lactation. *Physiol. Behav.* **14**, 705–710 (1975).
17. A. S. Clark, M. C. Kelton, F. A. Guarraci, E. Q. Clyons, Hormonal status and test condition, but not sexual experience, modulate partner preference in female rats. *Horm. Behav.* **45**, 314–323 (2004).
18. H. R. Phillipps, S. H. Yip, D. R. Grattan, Patterns of prolactin secretion. *Mol. Cell. Endocrinol.* **502**, 110679 (2020).
19. R. E. Harlan, B. D. Shivers, D. W. Pfaff, Midbrain microinfusions of prolactin increase the estrogen-dependent behavior, lordosis. *Science* **219**, 1451–1453 (1983).
20. J. A. Witcher, M. E. Freeman, The proestrous surge of prolactin enhances sexual receptivity in the rat. *Biol. Reprod.* **32**, 834–839 (1985).
21. S. D. Michael, Plasma prolactin and progesterone during the estrous cycle in the mouse. *Proc. Soc. Exp. Biol. Med.* **153**, 254–257 (1976).
22. Y. N. Sinha, C. B. Salocks, W. P. Vanderlaan, Prolactin and growth hormone levels in different inbred strains of mice: Patterns in association with estrous cycle, time of day, and perphenazine stimulation. *Endocrinology* **97**, 1112–1122 (1975).
23. R. S. E. Brown, M. Aoki, S. R. Ladyman, H. R. Phillipps, A. Wyatt, U. Boehm, D. R. Grattan, Prolactin action in the medial preoptic area is necessary for postpartum maternal nursing behavior. *Proc. Natl. Acad. Sci. U.S.A.* **114**, 10779–10784 (2017).
24. Y. Chen, A. Moutal, E. Navratilova, C. Kopruszinski, X. Yue, M. Ikegami, M. Chow, I. Kanazawa, S. S. Bellampalli, J. Xie, A. Patwardhan, K. Rice, H. Fields, A. Akopian, V. Neugebauer, D. Dodick, R. Khanna, F. Porreca, The prolactin receptor long isoform regulates nociceptor sensitization and opioid-induced hyperalgesia selectively in females. *Sci. Transl. Med.* **12**, eaay7550 (2020).
25. M. Aoki, P. Wartenberg, R. Grunewald, H. R. Phillipps, A. Wyatt, D. R. Grattan, U. Boehm, Widespread cell-specific prolactin receptor expression in multiple murine organs. *Endocrinology* **160**, 2587–2599 (2019).
26. R. S. Brown, I. C. Kokay, H. R. Phillipps, S. H. Yip, P. Gustafson, A. Wyatt, C. M. Larsen, P. Knowles, S. R. Ladyman, P. LeTissier, D. R. Grattan, Conditional deletion of the prolactin receptor reveals functional subpopulations of dopamine neurons in the arcuate nucleus of the hypothalamus. *J. Neurosci.* **36**, 9173–9185 (2016).
27. J. Li, T. Ishii, P. Feinstein, P. Mombaerts, Odorant receptor gene choice is reset by nuclear transfer from mouse olfactory sensory neurons. *Nature* **428**, 393–399 (2004).
28. J. W. Scott, D. W. Pfaff, Behavioral and electrophysiological responses of female mice to male urine odors. *Physiol. Behav.* **5**, 407–411 (1970).
29. B. Jemiolo, S. Harvey, M. Novotny, Promotion of the Whitten effect in female mice by synthetic analogs of male urinary constituents. *Proc. Natl. Acad. Sci. U.S.A.* **83**, 4576–4579 (1986).
30. M. V. Novotny, W. Ma, D. Wiesler, L. Zidek, Positive identification of the puberty-accelerating pheromone of the house mouse: The volatile ligands associating with the major urinary protein. *Proc. Biol. Sci.* **266**, 2017–2022 (1999).
31. P. Peele, I. Salazar, M. Mimmack, E. B. Keverne, P. A. Brennan, Low molecular weight constituents of male mouse urine mediate the pregnancy block effect and convey information about the identity of the mating male. *Eur. J. Neurosci.* **18**, 622–628 (2003).
32. K. Nishimura, K. Utsumi, M. Yuhara, Y. Fujitani, A. Iritani, Identification of puberty-accelerating pheromones in male mouse urine. *J. Exp. Zool.* **251**, 300–305 (1989).
33. H. M. Marsden, F. H. Bronson, Estrous synchrony in mice: Alteration by exposure to male urine. *Science* **144**, 1469 (1964).
34. J. A. Johansen, L. G. Clemens, A. A. Nunez, Characterization of copulatory behavior in female mice: Evidence for paced mating. *Physiol. Behav.* **95**, 425–429 (2008).
35. M. A. Farmer, A. Leja, E. Foxen-Craft, L. Chan, L. C. MacIntyre, T. Niaki, M. Chen, J. C. Mapplebeck, V. Tabry, L. Topham, M. Sukosd, Y. M. Binik, J. G. Pfaus, J. S. Mogil, Pain reduces sexual motivation in female but not male mice. *J. Neurosci.* **34**, 5747–5753 (2014).
36. L. J. Brunet, G. H. Gold, J. Ngai, General anosmia caused by a targeted disruption of the mouse olfactory cyclic nucleotide-gated cation channel. *Neuron* **17**, 681–693 (1996).
37. M. Paukert, A. Agarwal, J. Cha, V. A. Doze, J. U. Kang, D. E. Bergles, Norepinephrine controls astroglial responsiveness to local circuit activity. *Neuron* **82**, 1263–1270 (2014).
38. S. Wen, I. N. Gotze, O. Mai, C. Schauer, T. Leinders-Zufall, U. Boehm, Genetic identification of GnRH receptor neurons: A new model for studying neural circuits underlying reproductive physiology in the mouse brain. *Endocrinology* **152**, 1515–1526 (2011).
39. I. C. Kokay, A. Wyatt, H. R. Phillipps, M. Aoki, F. Ectors, U. Boehm, D. R. Grattan, Analysis of prolactin receptor expression in the murine brain using a novel prolactin receptor reporter mouse. *J. Neuroendocrinol.* **30**, e12634 (2018).
40. D. H. Brann, T. Tsukahara, C. Weinreb, M. Lipovsek, K. Van den Berge, B. Gong, R. Chance, I. C. Macaulay, H. J. Chou, R. B. Fletcher, D. Das, K. Street, H. R. de Bezieux, Y. G. Choi, D. Risso, S. Dudoit, E. Purdom, J. Mill, R. A. Hachem, H. Matsunami, D. W. Logan, B. J. Goldstein, M. S. Grubb, J. Ngai, S. R. Datta, Non-neuronal expression of SARS-CoV-2 entry genes in the olfactory system suggests mechanisms underlying COVID-19-associated anosmia. *Sci. Adv.* **6**, eabc5801 (2020).
41. K. J. Ressler, S. L. Sullivan, L. B. Buck, A zonal organization of odorant receptor gene expression in the olfactory epithelium. *Cell* **73**, 597–609 (1993).

42. S. L. Sullivan, M. C. Adamson, K. J. Ressler, C. A. Kozak, L. B. Buck, The chromosomal distribution of mouse odorant receptor genes. *Proc. Natl. Acad. Sci. U.S.A.* **93**, 884–888 (1996).
43. K. J. Ressler, S. L. Sullivan, L. B. Buck, Information coding in the olfactory system: Evidence for a stereotyped and highly organized epitope map in the olfactory bulb. *Cell* **79**, 1245–1255 (1994).
44. R. Vassar, S. K. Chao, R. Sitcheran, J. M. Nunez, L. B. Vosshall, R. Axel, Topographic organization of sensory projections to the olfactory bulb. *Cell* **79**, 981–991 (1994).
45. Y. Oka, K. Kobayakawa, H. Nishizumi, K. Miyamichi, S. Hirose, A. Tsuboi, H. Sakano, O-MACS, a novel member of the medium-chain acyl-CoA synthetase family, specifically expressed in the olfactory epithelium in a zone-specific manner. *Eur. J. Biochem.* **270**, 1995–2004 (2003).
46. F. Gussing, S. Bohm, NQO1 activity in the main and the accessory olfactory systems correlates with the zonal topography of projection maps. *Eur. J. Neurosci.* **19**, 2511–2518 (2004).
47. E. M. Norlin, M. Alenius, F. Gussing, M. Hagglund, V. Vedin, S. Bohm, Evidence for gradients of gene expression correlating with zonal topography of the olfactory sensory map. *Mol. Cell. Neurosci.* **18**, 283–295 (2001).
48. Y. Yoshihara, M. Kawasaki, A. Tamada, H. Fujita, H. Hayashi, H. Kagamiyama, K. Mori, OCAM: A new member of the neural cell adhesion molecule family related to zone-to-zone projection of olfactory and vomeronasal axons. *J. Neurosci.* **17**, 5830–5842 (1997).
49. J. Strotmann, S. Conzelmann, A. Beck, P. Feinstein, H. Breer, P. Mombaerts, Local permutations in the glomerular array of the mouse olfactory bulb. *J. Neurosci.* **20**, 6927–6938 (2000).
50. B. Zapiec, P. Mombaerts, Multiplex assessment of the positions of odorant receptor-specific glomeruli in the mouse olfactory bulb by serial two-photon tomography. *Proc. Natl. Acad. Sci. U.S.A.* **112**, E5873–E5882 (2015).
51. A. M. Maier, H. Breer, J. Strotmann, Structural features of an OR37 glomerulus: A comparative study. *Front. Neuroanat.* **11**, 125 (2017).
52. M. L. Schaefer, T. E. Finger, D. Restrepo, Variability of position of the P2 glomerulus within a map of the mouse olfactory bulb. *J. Comp. Neurol.* **436**, 351–362 (2001).
53. P. Mombaerts, F. Wang, C. Dulac, S. K. Chao, A. Nemes, M. Mendelsohn, J. Edmondson, R. Axel, Visualizing an olfactory sensory map. *Cell* **87**, 675–686 (1996).
54. M. B. Richard, S. R. Taylor, C. A. Greer, Age-induced disruption of selective olfactory bulb synaptic circuits. *Proc. Natl. Acad. Sci. U.S.A.* **107**, 15613–15618 (2010).
55. G. A. Graziadei, P. P. Graziadei, Neurogenesis and neuron regeneration in the olfactory system of mammals. II. Degeneration and reconstitution of the olfactory sensory neurons after axotomy. *J. Neurocytol.* **8**, 197–213 (1979).
56. J. W. Hinds, P. L. Hinds, N. A. McNelly, An autoradiographic study of the mouse olfactory epithelium: Evidence for long-lived receptors. *Anat. Rec.* **210**, 375–383 (1984).
57. A. Mackay-Sim, P. Kittel, Cell dynamics in the adult mouse olfactory epithelium: A quantitative autoradiographic study. *J. Neurosci.* **11**, 979–984 (1991).
58. S. Qiao, K. Nordstrom, L. Muijs, G. Gasparoni, S. Tierling, E. Krause, J. Walter, U. Boehm, Molecular plasticity of male and female murine gonadotropes revealed by mRNA sequencing. *Endocrinology* **157**, 1082–1093 (2016).
59. X. Ibarra-Soria, T. S. Nakahara, J. Lilue, Y. Jiang, C. Trimmer, M. A. Souza, P. H. Netto, K. Ikegami, N. R. Murphy, M. Kusma, A. Kirton, L. R. Saraiva, T. M. Keane, H. Matsunami, J. Mainland, F. Papes, D. W. Logan, Variation in olfactory neuron repertoires is genetically controlled and environmentally modulated. *eLife* **6**, e21476 (2017).
60. C. van der Linden, S. Jakob, P. Gupta, C. Dulac, S. W. Santoro, Sex separation induces differences in the olfactory sensory receptor repertoires of male and female mice. *Nat. Commun.* **9**, 5081 (2018).
61. S. W. Santoro, S. Jakob, Gene expression profiling of the olfactory tissues of sex-separated and sex-combined female and male mice. *Sci. Data* **5**, 180260 (2018).
62. J. Zhang, R. Pacifico, D. Cawley, P. Feinstein, T. Bozza, Ultrasensitive detection of amines by a trace amine-associated receptor. *J. Neurosci.* **33**, 3228–3239 (2013).
63. N. Kanageswaran, M. Nagel, P. Scholz, J. Mohrhardt, G. Gisselmann, H. Hatt, Modulatory effects of sex steroids progesterone and estradiol on odorant evoked responses in olfactory receptor neurons. *PLOS ONE* **11**, e0159640 (2016).
64. A. Fleischmann, B. M. Shykind, D. L. Sosulski, K. M. Franks, M. E. Glinka, D. F. Mei, Y. Sun, J. Kirkland, M. Mendelsohn, M. W. Albers, R. Axel, Mice with a "monoclonal nose": Perturbations in an olfactory map impair odor discrimination. *Neuron* **60**, 1068–1081 (2008).
65. M. Freemark, P. Driscoll, J. Andrews, P. A. Kelly, M. Royster, Ontogenesis of prolactin receptor gene expression in the rat olfactory system: Potential roles for lactogenic hormones in olfactory development. *Endocrinology* **137**, 934–942 (1996).
66. R. S. E. Brown, Z. Khant Aung, H. R. Phillipps, Z. Barad, H. J. Lein, U. Boehm, R. E. Szawka, D. R. Grattan, Acute suppression of LH secretion by prolactin in female mice is mediated by kisspeptin neurons in the arcuate nucleus. *Endocrinology* **160**, 1323–1332 (2019).
67. V. Hellier, O. Brock, M. Candlish, E. Desroziers, M. Aoki, C. Mayer, R. Piet, A. Herbison, W. H. Colledge, V. Prevot, U. Boehm, J. Bakker, Female sexual behavior in mice is controlled by kisspeptin neurons. *Nat. Commun.* **9**, 400 (2018).
68. Y. Sakuma, Neural substrates for sexual preference and motivation in the female and male rat. *Ann. N. Y. Acad. Sci.* **1129**, 55–60 (2008).
69. B. J. Le Boeuf, Interindividual associations in dogs. *Behaviour* **29**, 268–294 (1967).
70. K. Grammer, 5-α-androst-16en-3α-on: A male pheromone? A brief report. *Ethol. Sociobiol.* **14**, 201–207 (1993).
71. S. W. Gangestad, R. Thornhill, Menstrual cycle variation in women's preferences for the scent of symmetrical men. *Proc. Biol. Sci.* **265**, 927–933 (1998).
72. M. J. Rantala, C. J. P. Enksson, A. Vainikka, R. Kortet, Male steroid hormones and female preference for male body odor. *Evol. Hum. Behav.* **27**, 259–269 (2006).
73. I. Rodriguez, P. Feinstein, P. Mombaerts, Variable patterns of axonal projections of sensory neurons in the mouse vomeronasal system. *Cell* **97**, 199–208 (1999).
74. D. Kumar, M. Freese, D. Drexler, I. Hermans-Borgmeyer, A. Marquardt, U. Boehm, Murine arcuate nucleus kisspeptin neurons communicate with GnRH neurons in utero. *J. Neurosci.* **34**, 3756–3766 (2014).
75. M. Aoki, H. Takeuchi, A. Nakashima, H. Nishizumi, H. Sakano, Possible roles of Robo1+ ensheathing cells in guiding dorsal-zone olfactory sensory neurons in mouse. *Dev. Neurobiol.* **73**, 828–840 (2013).
76. A. Dobin, C. A. Davis, F. Schlesinger, J. Drenkow, C. Zaleski, S. Jha, P. Batut, M. Chaisson, T. R. Gingeras, STAR: Ultrafast universal RNA-seq aligner. *Bioinformatics* **29**, 15–21 (2013).
77. B. Li, C. N. Dewey, RSEM: Accurate transcript quantification from RNA-Seq data with or without a reference genome. *BMC Bioinformatics* **12**, 323 (2011).
78. M. D. Robinson, D. J. McCarthy, G. K. Smyth, edgeR: A Bioconductor package for differential expression analysis of digital gene expression data. *Bioinformatics* **26**, 139–140 (2010).
79. N. Romano, S. H. Yip, D. J. Hodson, A. Guillou, S. Parnaudeau, S. Kirk, F. Tronche, X. Bonnefont, P. Le Tissier, S. J. Bunn, D. R. Grattan, P. Mollard, A. O. Martin, Plasticity of hypothalamic dopamine neurons during lactation results in dissociation of electrical activity and release. *J. Neurosci.* **33**, 4424–4433 (2013).
80. T. Bozza, P. Feinstein, C. Zheng, P. Mombaerts, Odorant receptor expression defines functional units in the mouse olfactory system. *J. Neurosci.* **22**, 3033–3043 (2002).
81. L. Xu, W. Li, V. Voleti, D. J. Zou, E. M. C. Hillman, S. Firestein, Widespread receptor-driven modulation in peripheral olfactory coding. *Science* **368**, eaaz5390 (2020).
82. P. Pfister, B. C. Smith, B. J. Evans, J. H. Brann, C. Trimmer, M. Sheikh, R. Arroyave, G. Reddy, H. Y. Jeong, D. A. Raps, Z. Peterlin, M. Vergassola, M. E. Rogers, Odorant receptor inhibition is fundamental to odor encoding. *Curr. Biol.* **30**, 2574–2587.e6 (2020).
83. D. R. Reed, A. A. Bachmanov, M. G. Tordoff, Forty mouse strain survey of body composition. *Physiol. Behav.* **91**, 593–600 (2007).
84. C. I. Nussbaum-Krammer, M. F. Neto, R. M. Brielmann, J. S. Pedersen, R. I. Morimoto, Investigating the spreading and toxicity of prion-like proteins using the metazoan model organism C. elegans. *J. Vis. Exp.* 52321 (2015).
85. S. K. Tungtur, N. Nishimune, J. Radel, H. Nishimune, Mouse behavior tracker: An economical method for tracking behavior in home cages. *Biotechniques* **63**, 215–220 (2017).

Acknowledgments: In memory of Mari Aoki. **Funding:** This work was supported by grants from the German Science Foundation (Deutsche Forschungsgemeinschaft) through grants BO1743/9 and SFB 894 to U.B. **Author contributions:** M.A. and U.B. conceived the study. M.A., I.G., A.W., R.G., S.E.P., S.W., K.K., and G.G. conducted experiments and analyzed data. D.R.G., M.S.-T., O.H., S.Q., and J.W. provided experimental advice and important tools and reagents. M.A., A.W., D.R.G., and U.B. wrote the manuscript. **Competing interests:** The authors declare that they have no competing interests. **Data and materials availability:** All data needed to evaluate the conclusions in the paper are present in the paper and/or the Supplementary Materials. RNA-seq data generated in this study were deposited in the NCBI Sequence Read Archive (SRA) with the accession number PRJNA742660. External public data used in this study were GSE151346 and GSE112352. Further information and requests for resources and reagents should be directed to and will be fulfilled by the lead contact, U.B. (ulrich.boehm@uks.eu).

Submitted 4 January 2021
Accepted 19 August 2021
Published 8 October 2021
10.1126/sciadv.abg4074

Citation: M. Aoki, I. Gamayun, A. Wyatt, R. Grünewald, M. Simon-Thomas, S. E. Philipp, O. Hummel, S. Wagenpfeil, K. Kattler, G. Gasparoni, J. Walter, S. Qiao, D. R. Grattan, U. Boehm, Prolactin-sensitive olfactory sensory neurons regulate male preference in female mice by modulating responses to chemosensory cues. *Sci. Adv.* **7**, eabg4074 (2021).